Origin of Deformation Twinning in bcc Tungsten and Molybdenum

Jianwei Xiao,[1] Songwei Li,[1] Xiaoxiao Ma,[1] Junjie Gao,[1] Chuang Deng,[2] Zhaoxuan Wu,[1,3,*] and Yuntian Zhu[1,3,†]
[1]Department of Materials Science and Engineering, City University of Hong Kong, Hong Kong, China
[2]Department of Mechanical Engineering, University of Manitoba, Winnipeg, MB R3T 5V6, Canada
[3]Hong Kong Institute for Advanced Study, City University of Hong Kong, Hong Kong, China

(Received 7 January 2023; revised 8 June 2023; accepted 4 September 2023; published 26 September 2023)

Twinning is profuse in bcc transition metals (TMs) except bulk W and Mo. However, W and Mo nanocrystals surprisingly exhibit twinning during room temperature compression, which is completely unexpected as established nucleation mechanisms are not viable in them. Here, we reveal the physical origin of deformation twinning in W and Mo. We employ density functional theory (DFT) and a reduced-constraint slip method to compute the stress-dependent generalized stacking fault enthalpy (GSFH), the thermodynamic quantity to be minimized under constant loading. The simple slipped structures and GSFH lines show that compressive stresses stabilize a two-layer twin embryo, which can grow rapidly via twinning disconnections with negligible energy barriers. Direct atomistic simulations unveil the explicit twinning path in agreement with the DFT GSFH lines. Twinning is thus the preferred deformation mechanism in W and Mo when shear stresses are coupled with high compressive stresses. Furthermore, twinnability can be related to the elastic constants of a stacking fault phase (SFP). The hcp phase may serve as a candidate SFP for the $\{112\}\langle\bar{1}\,\bar{1}\,1\rangle$ twinning system in bcc TMs and alloys, which is coincident with the $\{111\}\langle 11\bar{2}\rangle$ twinning in fcc structures.

DOI: 10.1103/PhysRevLett.131.136101

Twinning plays an important role in plastic deformation of crystalline materials. Deformation twinning is ubiquitous in bcc Fe [1], V [2,3], Nb [4], Ta [2,4], and Cr [5] but is less active in bulk Mo and W under quasistatic loadings. The subtle differences among these elemental transition metals (TMs) were recently uncovered using a reduced-constraint (RC) slip method and associated γ_{rc} lines [6]. The RC slip allows multilayer interactions and atomic shuffle displacements, yielding γ_{rc} lines with identical or lower energies compared to the classical γ lines. The γ_{rc} line replaces the classical γ line and is applicable to both twin and dislocation nucleations in all crystal structures. For bcc TM in particular, γ_{rc} shows that a metastable two-layer twin embryo can be formed via a simple slip between two atom layers on the $\{112\}$ twinning plane in Fe, group VB TMs, and Cr, while coordinated slips of three atom layers are required to form a metastable three-layer twin embryo in Mo and W. Based on this twin nucleation path, twinning is naturally more difficult to activate in Mo and W. Nonetheless, twinning and detwinning are frequently reported in Mo and W nanocrystals upon loading and unloading at room temperature [7–9]. The activation of twinning was simply attributed to a lack of dislocation sources and higher stresses achievable in nanoscale samples [7]. However, many fundamental issues remain unclear in these two bcc elements, including the physical origin of twinning, the true twin nucleation path, effects of applied stresses, as well as the competition between twinning and dislocation plasticity [10,11].

In this Letter, we introduce the stress-dependent generalized stacking fault energy (GSFE) Ψ_U and enthalpy Ψ_H in Mo and W and show that the unstable two-layer twin embryo becomes metastable under compressive stresses above some threshold σ_c. The two-layer twin embryo, or the metastable stacking fault (SF), is nearly identical to that in other TMs. The presence of the metastable SF corroborates the profile of the generalized stacking fault enthalpy (GSFH), which is the quantity dictating thermodynamic equilibrium and twin nucleation under constant-stress loadings in small-scale samples [12]. Twin nucleation can thus occur in Mo and W via a simple slip similar to that in other bcc TMs. The barrier to reaching the metastable SF/twin embryo is lower than that required to nucleate a full dislocation. Twinning naturally becomes the favourable deformation mechanism over dislocation nucleation and glide. We present a simple, elasticity-based criterion as a *qualitative* condition for the metastability of the SF/two-layer twin embryo and show the twinning path in W via direct atomistic simulations.

The stress-dependent Ψ_U and Ψ_H are calculated using the RC slip method with a tilt cell [13–15] and density functional theory (DFT) as implemented in Vienna *Ab initio* Simulation Package [16,17] (Supplemental Material [18]). For a system with slip $\mathbf{s}$ and under normal stress σ_n, its internal energy U is a state function completely determined by two state variables $\mathbf{s}$ and l, i.e., $U(\mathbf{s}, l)$, where l is the system length in the slip plane normal. On the $\{112\}$ twinning plane, $\mathbf{s}$ is always along $\langle 111\rangle$ and can be

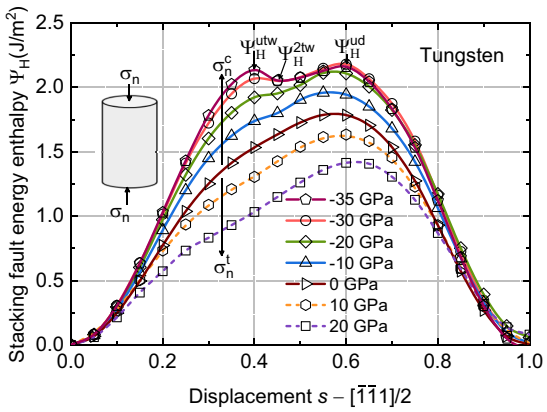

FIG. 1. The GSFH $\Psi_H(\mathbf{s}, \sigma_n)$ on the $\{112\}$ twinning plane of bcc W structures calculated as a function of σ_n using DFT.

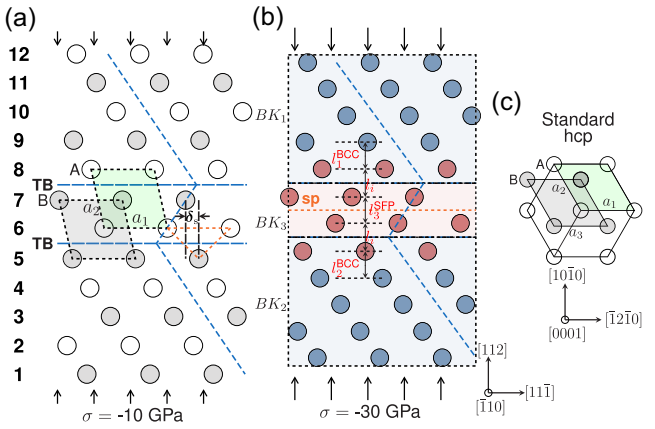

FIG. 2. SF structure computed for W by DFT. (a) A metastable SF/two-layer twin embryo at $\mathbf{s} \approx 0.45\mathbf{b}$ under $\sigma_n = -10$ GPa. (b) Local atomic environment at $\sigma_n = -30$ GPa by common neighbor analysis (CNA) [48]: blue denotes bcc; red denotes hcp. (c) hcp unit cell viewed along [0001].

denoted by slip distance s. Treating s and l as control variables, the *total differential* (d) of U is

$$dU(s,l) = \tau A ds + \sigma_n A dl, \tag{1}$$

where τ is the shear stress and A is the slip-plane cross-sectional area. Applying the Legendre transformation to $U(s,l)$, we obtain the enthalpy and its total differential as

$$H(s,\sigma_n) = U - \sigma_n A l; \tag{2}$$

$$dH(s,\sigma_n) = \tau A ds - l A d\sigma_n. \tag{3}$$

The stress-dependent GSFE and GSFH can be defined as [12]

$$\Psi_U(s,\sigma_n) = [U(s,\sigma_n) - U(0,\sigma_n)]/A \quad \text{and} \tag{4}$$

$$\Psi_H(s,\sigma_n) = [H(s,\sigma_n) - H(0,\sigma_n)]/A = \Psi_U - \sigma_n \Delta l(s,\sigma_n), \tag{5}$$

where $\Delta l = l(s,\sigma_n) - l(0,\sigma_n)$ is the slip-induced displacement in the slip plane normal. In the above, $U(s,l)$ can be computed directly in DFT or atomistic simulations. In the RC slip process, the system is under constant σ_n. The final equilibrium structure thus minimizes the system enthalpy $H(s,\sigma_n) = A\Psi_H(s,\sigma_n) + H(0,\sigma_n)$. For each σ_n, A and $H(0,\sigma_n)$ are constant, $\Psi_H(s,\sigma_n)$ is the critical quantity to minimize.

Figure 1 shows the $\Psi_H(s,\sigma_n)$ for W (Mo in Supplemental Material [18]). For both elements, Ψ_H increases or decreases under compression or tension. A local energy valley or metastable SF first appears when $\sigma_n \leq -10$ GPa and -5 GPa for W and Mo, respectively, indicating that the simple slipped configuration is stable against perturbations in s near $s \approx 0.45|\mathbf{b}|$, where $\mathbf{b} = \langle 111 \rangle/2$ is the lattice Burgers vector. Furthermore, the barrier Ψ_H^{utw} to the SF is close but lower than Ψ_H^{ud} for completing the slip and forming the full dislocation. High compressive stresses thus change the Ψ_H profiles of W and Mo to that of Ψ_U of other bcc TMs and stabilize the SF, which at least provides the basis structure for twin nucleation and growth via subsequent slips on consecutive $\{112\}$ planes [6,47]. Below the threshold σ_n, no metastable point is seen and the formed SF is *unstable*. The metastable SF never appeared in any $\Psi_U(s,\sigma_n)$ line (see Supplemental Material [18]).

Figure 2 shows the optimized structures in W upon removal of all ionic constraints (σ_n is kept constant). At low compressive stresses ($\sigma_n > -10$ GPa), the slipped structure is unstable and falls back to perfect bcc, consistent with the lack of metastable SF on respective Ψ_H lines. At high compressive stresses ($\sigma_n \leq -10$ GPa), the slipped structure is stable; the SF region consists of four atom layers resembling a two-layer twin embryo similar to that in other bcc TMs at $\sigma_n = 0$ [Figs. 2(a) and 2(b) and Ref. [6]]. The formed twin embryo is enclosed by two near-isosceles twin boundaries (TBs); each TB is characterized by a displacement $\boldsymbol{\delta}_s$ along the twinning direction (between layers 5 and 6, 7 and 8) and a displacement $\boldsymbol{\delta}_n$ perpendicular to the twinning plane (see Supplemental Material [18]). These local displacements vary among atom layers above and below the slip plane, and are only captured in the RC slip method. In the twinning direction, the critical slip $s \approx 0.45|\mathbf{b}|$ to the formation of the twin embryo is reached earlier than $s \approx 0.6|\mathbf{b}|$ to the full dislocation. Twinning is thus expected to be activated first under shear coupled with high compressive loadings. In addition, atoms above and below the isosceles TBs have a local atomic environment similar to that in hcp structures (see Supplemental Material [18]). Specifically, the bcc $\{112\}$ plane has the same atomic arrangement as that of the hcp $\{10\bar{1}0\}$ plane. At $\mathbf{s} \approx 0.45\mathbf{b}$, the four layers of atoms on the bcc $\{112\}$ plane

form four hcp $\{10\bar{1}0\}$-like atom planes. The structure transformation is achieved by the displacement $\boldsymbol{\delta}_s$ driven by high compressive σ_n in Mo and W; similar displacements occur spontaneously in other bcc TMs without σ_n. The stabilization of the two-layer twin embryo enables relatively easy twin growth via TB disconnections (see below and Supplemental Material [18]). The critical stress $\sigma_n^c \approx -10$ GPa to stabilize the twin embryo is similar to that in compression of W nanocrystals [7,8].

While the four-layer SF region does not have an exact hcp structure, its close resemblance may allow qualitative relation to be established between the metastable SF/two-layer twin embryo and the hcp structure. To test this hypothesis, we treat the two-layer twin embryo as a stacking fault phase (SFP) of finite thickness (two layers), in contrast to the conventional slip fault of zero thickness. We derive the GSFE and GSFH expressions using a sandwiched structure consisting of two bcc regions, one SFP region, and two TB interfaces [Fig. 2(b)]. Following Eq. (4), the GSFE is

$$A\Psi_U(s,\sigma_n) = U_3^{SFP}(s,\sigma_n) - U_3^{bcc}(0,\sigma_n) + 2A\gamma_i(s,\sigma_n), \quad (6)$$

where U_3 is the internal energy of the SFP/bcc region, γ_i is the interface energy between the bcc bulk and SFP during slip. Ψ_U can be computed exactly in DFT or atomistic simulations.

The change of l in GSFH of Eq. (5) can be approximated as

$$\Delta l(s,\sigma_n) = l_3^{SFP}(s,\sigma_n) + 2l_i(s,\sigma_n) - 3l_{\{112\}}^{bcc}(0,\sigma_n), \quad (7)$$

where l_3^{SFP} and l_i are the stress- and slip-dependent interplanar distances in the SFP and interfaces, and $l_{\{112\}}^{bcc}$ is the stress-dependent bcc $\{112\}$ plane interplanar distance (see Supplemental Material [18]). Finally, the GSFH can be expressed as

$$\Psi_H(s,\sigma_n) = \left[H_3^{SFP}(s,\sigma_n) - H_3^{bcc}(0,\sigma_n)\right]/A + 2\gamma_i(s,\sigma_n) - \sigma_n\left[2l_i(s,\sigma_n) - 2l_{\{112\}}^{bcc}(0,\sigma_n)\right]. \quad (8)$$

The presence of the metastable SF requires

$$\left(\frac{\partial^2\Psi_H}{\partial s^2}\right)_{\sigma_n} > 0; \qquad \left(\frac{\partial\Psi_H}{\partial s}\right)_{\sigma_n} = 0. \quad (9)$$

For small perturbations of s, the stability condition is

$$\left(\frac{\partial^2\Psi_H}{\partial s^2}\right)_{\sigma_n} = \frac{1}{A}\left(\frac{\partial^2 H_3^{SFP}}{\partial s^2}\right)_{\sigma_n} + 2\left(\frac{\partial^2\gamma_i(s,\sigma_n)}{\partial s^2}\right)_{\sigma_n} - 2\sigma_n\left(\frac{\partial^2 l_i(s,\sigma_n)}{\partial s^2}\right)_{\sigma_n} > 0. \quad (10)$$

The analysis is conceptually general up to this stage. However, the partition of the SF energy into the SFP bulk and interfaces is not quantitatively rigorous since the SFP is only two atom layers surrounded by two additional layers in similar local environments. Nonetheless, this approach allows us to relate the sandwiched SF properties to the computable properties of the SFP bulk and TBs.

Since the slip is localized along the slip plane only, we may further assume that the interface energy $\gamma_i(s,\sigma_n)$ and length $l_i(s,\sigma_n)$ are less sensitive (second-order effects) to small perturbations in s than H_3^{SFP}. In this case, the stability condition becomes

$$\left(\frac{\partial^2\Psi_H}{\partial s^2}\right)_{\sigma_n} \approx \frac{1}{A}\left(\frac{\partial^2 H_3^{SFP}}{\partial s^2}\right)_{\sigma_n}. \quad (11)$$

This step is perhaps a broad simplification but again is necessary to relate the stability of the twin embryo to the SFP properties. The total differential of the SFP enthalpy can be written as

$$dH_3^{SFP} = \tau A ds - l_3^{SFP} A d\sigma_n. \quad (12)$$

The stability condition of the twin embryo is thus

$$\left(\frac{\partial^2\Psi_H}{\partial s^2}\right)_{\sigma_n} = A\left(\frac{\partial\tau}{\partial s}\right)_{\sigma_n} > 0. \quad (13)$$

Considering a Cartesian coordinate system with x_1, x_2, and x_3 in the slip direction, slip direction normal, and the slip plane normal, infinitesimal slip ds can be written as $\varepsilon_5 = ds/l_3^{SFP}$. The stability condition is simplified to

$$\left(\frac{\partial^2\Psi_H}{\partial s^2}\right)_{\sigma_n} = l_3^{SFP}\left(\frac{\partial\sigma_5}{\partial\varepsilon_5}\right)_{\sigma_3,\varepsilon_1,\varepsilon_2,\varepsilon_4,\varepsilon_6} > 0, \quad (14)$$

where the derivative is taken at constant σ_3, ε_1, ε_2, ε_4, ε_6 following the loading conditions imposed in computing Ψ_H.

Assuming linear elasticity at infinitesimal strain ε_5 and using the σ_3-stressed system as a reference, the change of stress can be obtained by Hooke's law as

$$\Delta\sigma_i = \sigma_i - \sigma_i^{ref} = C_{ij}\varepsilon_j, \quad (15)$$

where σ_i is the final stress and σ_i^{ref} is the stress in the reference state. Applying the condition $\Delta\sigma_3 = 0$ and $\varepsilon_1 = \varepsilon_2 = \varepsilon_4 = \varepsilon_6 = 0$, we obtain

$$\Delta\sigma_5 = \left(C_{33}C_{55} - C_{35}^2\right)\varepsilon_5/C_{33}. \quad (16)$$

The stability condition in Eq. (14) can be denoted using a twinnability index ω defined in terms of the elastic constants of the bulk SFP as

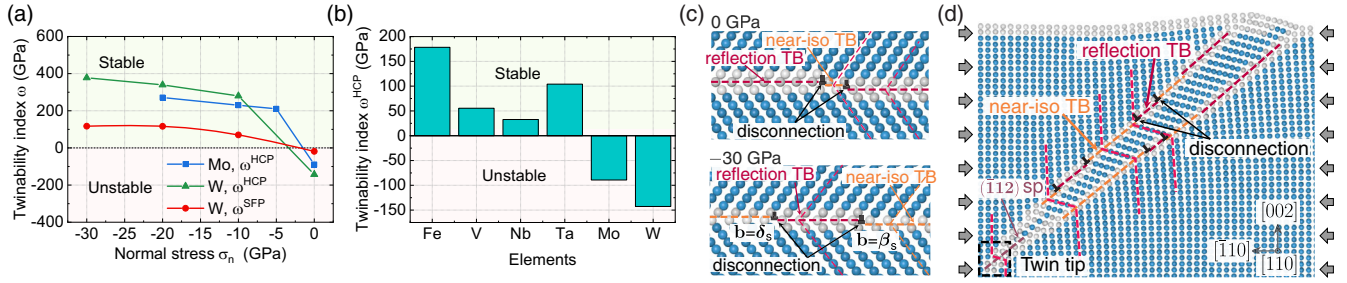

FIG. 3. Twinnability index ω and twin nucleation and growth under compression σ_n. (a) ω calculated by the elastic constants of the SFP and hcp surrogates for W and Mo using DFT. The SFP/hcp structure is stabilized ($C_{11} > C_{12}$) at high compressive σ_n. (b) ω for six bcc transition metals at zero σ_n using their respective hcp elastic constants computed by DFT [50]. (c) Change of TB from the mirror reflection at zero σ_n to the near-isosceles structure with a dissociated disconnection at $\sigma_n = -30$ GPa. (d) Twin nucleation by a simple shear at the twin tip and subsequent growth by dissociated disconnections in compression of W single crystal in 300 K MD simulations. In (c),(d), atoms are colored by their local atomic environment identified by CNA [48]; blue denotes bcc; white denotes others.

$$\omega^{\mathrm{SFP}} = \frac{\partial^2 \Psi_{\mathrm{H}}}{\partial s^2}_{\sigma_n} = \frac{C_{33}C_{55} - C_{35}^2}{C_{33}} > 0. \tag{17}$$

For W and Mo, we can treat the SFP as hcp and ω^{SFP} is then

$$\omega^{\mathrm{hcp}} = \frac{1}{2}\left(C_{11}^{\mathrm{hcp}} - C_{12}^{\mathrm{hcp}}\right) > 0, \tag{18}$$

where C_{ij}^{hcp} is the elastic constant in the *standard* hcp unit cell. Under large uniaxial stresses, the reduced index ω^{hcp} is less well defined since the hcp structure and its elastic property lose symmetry and ω^{SFP} should be used instead.

We now provide validations on the above stability conditions. Since the relation in Eq. (17) is general, we first consider the $\{111\}$ plane GSFE Ψ_{U} lines in elemental fcc metals where the stacking fault has an exact local hcp structure at slip $s = \langle 11\bar{2}\rangle/6$. In this case, $\omega^{\mathrm{SFP}} = C_{44}^{\mathrm{hcp}}$. Among nine fcc metals (Ag, Al, Au, Cu, Ir, Ni, Pd, Pt, Rh), all except Pt exhibit a clearly well-defined metastable SF with a positive curvature on DFT-based $\Psi_{\mathrm{U}}(s, 0)$ at $s \approx \langle 11\bar{2}\rangle/6$ [49], consistent with the fact that all except Pt have their $C_{44}^{\mathrm{hcp}} > 0$ [50]. We next examine the $\Psi_{\mathrm{U}}(s, 0)$ profiles of bcc Ti which is unstable at 0 K. For all three slip planes ($\{110\}$, $\{112\}$, and $\{123\}$), the stability indices ω^{SFP} can be calculated using the elastic constants of the bcc structure. In this case, all ω^{SFP} are small and approach zero, and the curvatures of the respective Ψ_{U} approach zero, again consistent with the stability criterion (see Supplemental Material [18]).

The above two cases have their SFP structures represented exactly by elemental structures and should have the best agreement between ω and the presence of metastable points on Ψ_{U}. For the bcc twinnability, we focus on the domain where the SF is metastable and the SFP only resembles the hcp structure, i.e., $s \approx 0.45|\mathbf{b}|$ and $\sigma_n \leq -10$ GPa in the current study. Figure 3(a) shows ω as a function of normal stresses in W and Mo. At low stresses, the elastic constants are calculated based on affine transformation without optimizing ion positions. This constrained calculation is not ideal but necessary since the hcp and SFP structures are mechanically unstable ($C_{11} < C_{12}$, $C_{44} < 0$) in these two elements. The stability conditions in Eq. (17) and Eq. (18) are not satisfied in both W and Mo. On the other hand, high compressive stresses stabilize both the hcp and SFP structures, leading to $\omega > 0$ and meeting the stability requirement (see Supplemental Material [18]). Overall, the stress-driven stabilization of the hcp/SFP is consistent with the stability of the SF on the respective Ψ_{H} lines.

The stability condition can also be applied in group VB TMs and Fe. Figure 3(b) shows the twinnability index ω^{hcp} based on C^{hcp} at stress-free conditions by DFT [50]. Group VB TMs and Fe have $\omega^{\mathrm{hcp}} > 0$, satisfying the stability criterion and in agreement with the presence of a metastable point on their Ψ_{U} and the two-layer twin embryo at stress-free conditions [6].

For Mo and W, the critical stresses cannot be determined precisely using either ω^{SFP} or ω^{hcp}, nor is the current simplistic model expected to give quantitative prediction. Comparing the SFP/hcp model and the true sandwiched SF, the largest discrepancies perhaps arise from the small thickness of the SFP and the structure differences between the hcp and SFP. To illustrate this point, we calculated the elastic constants of the SFP and the hcp surrogate and found non-negligible, quantitative differences in their elastic constants and thus the critical compressive stress satisfying the stability condition (see Supplemental Material [18]). In addition, direct calculation of Ψ_{H} with an interatomic potential [51] shows that the presence of the metastable SF is also sensitive to other stress component (e.g., σ_{xz}, Supplemental Material [18]). Nonetheless, in all of the cases, the metastable SF/two-layer twin embryo is only stabilized at high compressive stresses which in turn favor twinnability. The twinnability index can also be changed via alloying, as demonstrated in binary TaRe and WRe alloys (see Supplemental Material [18]). Further

predictions in medium/high entropy alloys show qualitative agreements with extant experiments.

Finally, we demonstrate the simple-slip twin nucleation mechanism under compression using direct molecular dynamics (MD) simulations with a spline modified embedded-atom method (MEAM) potential for W [51]. This potential reproduces critical features of DFT $\Psi_H(s, \sigma_n)$ for W (see Supplemental Material [18]). Figure 3(c) shows the structures of the TB and TB disconnections. At zero normal stress, the TB has a reflection mirror symmetry in agreement with that in DFT and its Ψ_U profile. The TB disconnection has a compact core with width similar to $|\mathbf{b}|$. With increasing normal stresses σ_n, the TB transforms from mirror reflection to a near-isosceles structure. The TB disconnection dissociates into a pair of partial disconnections of Burgers vectors $\boldsymbol{\delta}_s$ and $\boldsymbol{\beta}_s$ satisfying $\boldsymbol{\delta}_s + \boldsymbol{\beta}_s = \mathbf{b}_t$ (see Ref. [6] for details). In between the two partials, the TB adopts the mirror structure, akin to SFs between Shockley partial pairs in fcc structures. High compressive stresses thus reverse the stability of the reflection and mirror TBs, fully consistent with the DFT results in Fig. 2.

Figure 3(d) shows the nucleation and growth of a twin in a pillar compressed along $\langle 110 \rangle$ at 300 K (see Supplemental Material [18]). Upon reaching the critical loading of 30 GPa (~20 GPa in experiments [7]), a deformation twin nucleates from the free surface. The nucleation is carried out by slip between two $\{112\}$-plane atom layers, leading to the formation of a two-layer twin embryo as in the RC slip [Figs. 2(a) and 2(b)]. At the twin tip, the localized slip advances quickly towards the pillar center via a partial dislocation $\mathbf{b}_s$. The propagation of the slip is simultaneously accompanied by twin thickening on both sides of the twin embryo. The thickening process is carried out by the nucleation and glide of partial twinning disconnections of Burgers vectors $\boldsymbol{\delta}_s$ and $\boldsymbol{\beta}_s$ separated by some TB segments of reflection symmetry. No dislocation is observed in the entire compression process. Therefore, under high compressive stresses, the barrier to twinning is lower than that to dislocation nucleation; twinning is the preferred deformation mechanism. The twin nucleation and growth process in W is similar to that in other bcc TMs exhibiting a metastable SF/two-layer twin embryo under stress-free conditions [6]. Further discussion is provided on the competition and prediction of critical conditions of twinning (similar to that in fcc structures [10,11]), their temperature dependence, and limitations in large-scale systems in the Supplemental Material [18].

In summary, the origin of deformation twinning in bcc W and Mo is revealed by considering stress-dependent GSFH. Stresses can change both the value and the profile of GSFH. The profile change dictates the metastability of twin embryos, which has not been widely recognized, but may be general to other bcc TMs. For Mo and W, high compressive stresses stabilize the previous unstable stacking fault/two-layer twin embryo on the $\{112\}$ twinning plane. Above the critical stresses, twin nucleation can occur via a simple slip between two atom planes as in other bcc TMs. Stress affects both the twin nucleation and growth paths, as well as the TB structures and disconnections. This mechanistic understanding rationalizes a wide range of extant experiments on deformation of Mo and W at small scales. The present study thus provides a unified twin nucleation mechanism and a computational method for quantitative determination of twinning path and barriers applicable to all bcc structures.

This work is supported by the National Key R&D Program of China (2021YFA1200202), the Research Grants Council, Hong Kong SAR through the Early Career Scheme Fund (CityU 21205019) and the Collaborative Research Fund (C1005-19G), and the National Natural Science Foundation of China (51931003). Computational resources are provided by Compute Canada and CityU Burgundy, managed and provided by the Computing Services Centre at City University of Hong Kong.

*Corresponding author: zhaoxuwu@cityu.edu.hk
†Corresponding author: y.zhu@cityu.edu.hk

[1] A. T. Churchman and A. H. Cottrell, Nature (London) **167**, 943 (1951).
[2] Y. M. Wang, A. M. Hodge, J. Biener, A. V. Hamza, D. E. Barnes, K. Liu, and T. G. Nieh, Appl. Phys. Lett. **86**, 101915 (2005).
[3] R. Gröger, Z. Chlup, and T. Kuběnové, Mater. Sci. Eng. **737**, 413 (2018).
[4] B. Jiang, A. Tu, H. Wang, H. Duan, S. He, H. Ye, and K. Du, Acta Mater. **155**, 56 (2018).
[5] J. Holzer, Z. Chlup, T. Kruml, and R. Gröger, Int. J. Plast. **138**, 102938 (2021).
[6] J. Xiao, L. Zhu, R. Wang, C. Deng, Z. Wu, and Y. Zhu, Mater. Today **65**, 90 (2023).
[7] J. Wang, Z. Zeng, C. R. Weinberger, Z. Zhang, T. Zhu, and S. X. Mao, Nat. Mater. **14**, 594 (2015).
[8] X. Wang, J. Wang, Y. He, C. Wang, L. Zhong, and S. X. Mao, Nat. Commun. **11**, 2497 (2020).
[9] X. Li, Q. Zeng, and J. Wang, Scr. Mater. **220**, 114930 (2022).
[10] E. B. Tadmor and S. Hai, J. Mech. Phys. Solids **51**, 765 (2003).
[11] E. B. Tadmor and N. Bernstein, J. Mech. Phys. Solids **52**, 2507 (2004).
[12] P. Andric, B. Yin, and W. A. Curtin, J. Mech. Phys. Solids **122**, 262 (2019).
[13] J. A. Nieminen, A. P. Sutton, and J. B. Pethica, Acta Metall. Mater. **40**, 2503 (1992).
[14] A. P. Sutton and R. W. Balluffi, *Interfaces in Crystalline Materials* (Clarendon Press, Oxford, 1995).
[15] S. Kibey, J. B. Liu, D. D. Johnson, and H. Sehitoglu, Appl. Phys. Lett. **89**, 191911 (2006).
[16] G. Kresse and J. Furthmüller, Phys. Rev. B **54**, 11169 (1996).

[17] G. Kresse and D. Joubert, Phys. Rev. B **59**, 1758 (1999).
[18] See Supplemental Material at http://link.aps.org/supplemental/10.1103/PhysRevLett.131.136101, which include Refs. [19–46], for more details on methods and validations.
[19] J. P. Perdew, K. Burke, and M. Ernzerhof, Phys. Rev. Lett. **77**, 3865 (1996).
[20] P. E. Blöchl, Phys. Rev. B **50**, 17953 (1994).
[21] M. Methfessel and A. T. Paxton, Phys. Rev. B **40**, 3616 (1989).
[22] H. J. Monkhorst and J. D. Pack, Phys. Rev. B **13**, 5188 (1976).
[23] A. P. Thompson, H. M. Aktulga, R. Berger, D. S. Bolintineanu, W. M. Brown, P. S. Crozier, P. J. in't Veld, A. Kohlmeyer, S. G. Moore, T. D. Nguyen *et al.*, Comput. Phys. Commun. **271**, 108171 (2022).
[24] M.-C. Marinica, L. Ventelon, M. R. Gilbert, L. Proville, S. L. Dudarev, J. Marian, G. Bencteux, and F. Willaime, J. Phys. Condens. Matter **25**, 395502 (2013).
[25] R. Wang, L. Zhu, S. Pattamatta, S. D. J., and Z. Wu, arXiv:2209.12323.
[26] C. Kittel, *Introduction to Solid State Physics* (Wiley, New York, 2005).
[27] G. Simmons and H. Wang, *Single Crystal Elastic Constants and Calculated Aggregate Properties: A Handbook*, 2nd ed. (The MIT Press, Cambridge, MA, 1971).
[28] Y. Su, S. Xu, and I. J. Beyerlein, J. Appl. Phys. **126**, 105112 (2019).
[29] T. Wen, R. Wang, L. Zhu, L. Zhang, H. Wang, D. J. Srolovitz, and Z. Wu, npj Comput. Mater. **7**, 206 (2021).
[30] R. G. Hennig, T. J. Lenosky, D. R. Trinkle, S. P. Rudin, and J. W. Wilkins, Phys. Rev. B **78**, 054121 (2008).
[31] R. Wang, X. Ma, L. Zhang, H. Wang, D. J. Srolovitz, T. Wen, and Z. Wu, Phys. Rev. Mater. **6**, 113603 (2022).
[32] J. R. Rice, J. Mech. Phys. Solids **40**, 239 (1992).
[33] R. J. Asaro and S. Suresh, Acta Mater. **53**, 3369 (2005).
[34] Extended modified embedded-atom method implementation in LAMMPS (accessed 15 August 2022), https://gitlab.com/CompMatSci/xmeam.
[35] Y. Mishin, M. J. Mehl, D. A. Papaconstantopoulos, A. F. Voter, and J. D. Kress, Phys. Rev. B **63**, 224106 (2001).
[36] T. C. Ting, *Anisotropic Elasticity: Theory and Applications* (Oxford University Press, New York, 1996).
[37] Y. Sun and G. E. Beltz, J. Mech. Phys. Solids **42**, 1905 (1994).
[38] P. Andric and W. Curtin, J. Mech. Phys. Solids **113**, 144 (2018).
[39] P. Andric and W. Curtin, J. Mech. Phys. Solids **106**, 315 (2017).
[40] L. Nordheim, Ann. Phys. (Berlin) **401**, 607 (1931).
[41] L. Bellaiche and D. Vanderbilt, Phys. Rev. B **61**, 7877 (2000).
[42] J. Shields, S. Goods, R. Gibala, and T. Mitchell, Mater. Sci. Eng. **20**, 71 (1975).
[43] X. Yan and Y. Zhang, Scr. Mater. **178**, 329 (2020).
[44] M. Wu, S. Wang, F. Xiao, G. Zhu, C. Yang, D. Shu, and B. Sun, J. Mater. Sci. Technol. **110**, 210 (2022).
[45] O. N. Senkov, J. M. Scott, S. V. Senkova, F. Meisenkothen, D. B. Miracle, and C. F. Woodward, J. Mater. Sci. **47**, 4062 (2012).
[46] Y. Sun, G. E. Beltz, and J. R. Rice, Mater. Sci. Eng. **170**, 67 (1993).
[47] S. Ogata, J. Li, and S. Yip, Phys. Rev. B **71**, 224102 (2005).
[48] D. Faken and H. Jónsson, Comput. Mater. Sci. **2**, 279 (1994).
[49] A. Hunter, R. F. Zhang, and I. J. Beyerlein, J. Appl. Phys. **115**, 134314 (2014).
[50] S. Shang, A. Saengdeejing, Z. Mei, D. Kim, H. Zhang, S. Ganeshan, Y. Wang, and Z. Liu, Comput. Mater. Sci. **48**, 813 (2010).
[51] H. Park, M. Fellinger, T. Lenosky, W. Tipton, D. Trinkle, S. P. Rudin, C. Woodward, J. Wilkins, and R. Hennig, MEAM potential for W developed by Park *et al.* (2012) v001 (2021), https://openkim.org/id/MO_560940542741_001.